Research Square

Preprints are preliminary reports that have not undergone peer review.
They should not be considered conclusive, used to inform clinical practice,
or referenced by the media as validated information.

Ferulic acid ameliorates neuroinflammation and cognitive deficits in Alzheimer's disease via the mGluR5/CaMKII/NF-κB pathway

Ting Yu
Hangzhou Medical College
Jian Zhang
Hangzhou Medical College
Yuanyuan Wang
Hangzhou Medical College
Zhou Shu
Hangzhou Medical College
Wen Liu
Hangzhou Medical College
Yuhao Wu
Hangzhou Medical College
Lichun Zhou
Hangzhou Medical College
Qiuran Xu
Hangzhou Medical College
Yingjun Li
Hangzhou Medical College
Yuanxiao Yang
Yujung@hmc.edu.cn
Hangzhou Medical College

Research Article

Keywords: Ferulic acid, Alzheimer's disease, mGluR5/CaMKII/NF-κB, Neuroinflammation, Microglia

Posted Date: April 9th, 2026

DOI: https://doi.org/10.21203/rs.3.rs-9200629/v1

License: This work is licensed under a Creative Commons Attribution 4.0 International License.
Read Full License

Additional Declarations: No competing interests reported.

Abstract

Background Alzheimer's disease (AD) is a progressive neurodegenerative disorder in which neuroinflammation plays a critical pathogenic role. Ferulic acid (FA), a natural phenolic compound widely distributed in plants, has been increasingly reported to exert potent neuroprotective effects. However, the specific molecular mechanism underlying the neuroprotective effects of FA in AD remains unclear, which limits its further development and application as a potential therapeutic agent for AD.

Objectives The present study aimed to investigate the therapeutic effects of FA on AD and clarify its underlying molecular mechanism, focusing on the mGluR5/CaMKII/NF-κB pathway and its association with microglia-mediated neuroinflammation.

Methods 3×Tg-AD mice and LPS-induced BV2 cells were used as experimental models to explore the effects of FA. Multiple experimental techniques were employed for comprehensive analyses, including immunofluorescence, flow cytometry, Nissl staining, HE staining, and western blot. These methods were used to detect mGluR5/CaMKII/NF-κB pathway protein levels, inflammatory factor formation, microglial activation, and pathological changes in AD models.

Results In 3×Tg-AD mice, FA treatment significantly increased the protein level of mGluR5, ameliorated neuroinflammation, and reduced Aβ plaque deposition in the brain as well as p-tau levels in the plasma. In LPS-stimulated BV2 cells, FA treatment decreased the formation of the pro-inflammatory factors and alleviated the over-activation of microglia. Further analyses confirmed that FA-induced up-regulation of mGluR5 inhibited the CaMKII/NF-κB signaling cascade, which in turn suppressed neuroinflammation and ameliorated cognitive deficits.

Conclusion These results demonstrated that FA exerts neuroprotective effects in AD as a specific mGluR5 agonist. The underlying mechanism is related to the regulation of the mGluR5/CaMKII/NF-κB pathway, which suppresses microglia-mediated neuroinflammation and ultimately ameliorates cognitive impairment. This study provides novel insights into the molecular mechanism of FA in AD treatment and highlights its promising potential as a candidate therapeutic agent for AD.

Introduction

Alzheimer's disease (AD) is a progressive neurodegenerative disorder characterized by core clinical hallmarks of cognitive impairment and memory deficits [1]. Microglial activation has been widely recognized as an early pathogenic event in AD, given its occurrence prior to the onset of mild cognitive impairment (MIC) and even before the formation and deposition of β-amyloid (Aβ) plaques. As the main immune effector cells in the central nervous system(CNS), microglia are essential for maintaining the homeostasis of CNS [2, 3]. Dysfunction of microglia can lead to excessive release of pro-inflammatory cytokines, and promote the aggregation and deposition of Aβ plaques, which subsequently impairs the survival and function of neurons, ultimately accelerating the deterioration of cognitive and function in AD

[4, 5]. Therefore, it is crucial to conduct research on the key proteins that regulate the homeostasis of microglia during the early stages of AD.

Metabotropic glutamate receptor 5 (mGluR5), a member of group I metabotropic glutamate receptors (mGluRs), is a G protein-coupled receptor (GPCR) that plays a pivotal role in regulating glutamatergic neurotransmission, synaptic plasticity, and cognitive processes [6, 7]. mGluR5 is highly expressed in brain regions crucial for learning and memory, such as the hippocampus and cerebral cortex, which are the core areas of cognitive function and neuroinflammation related to AD [8, 9]. Recent and clinical studies have shown that mGluR5 plays a crucial role in the pathological mechanism of AD. Specifically, its alterations in glial cells trigger the activation of downstream pro-inflammatory signaling pathways, resulting in excessive release of pro-inflammatory cytokines and chemokines. This pro-inflammatory cascade reaction further exacerbates neuronal damage, impairs synaptic function, and disrupts the balance between the production and clearance of Aβ in AD [10, 11]. The activated mGluR5 will activate phospholipase C (PLC), which subsequently leads to the release of intracellular calcium ions (Ca^{2+}) and the activation of calcium/calmodulin-dependent protein kinase II (CaMKII) [12]. Activated CaMKII participates in multiple AD-related cellular processes, including neuroinflammation, Aβ metabolism, and tau phosphorylation [13, 14]. Previous studies have demonstrated abnormal activation of CaMKII in AD patient brain tissues. Moreover, CaMKII interacts with nuclear factor-κB (NF-κB), a key transcription factor regulating proinflammatory cytokine expression and central to AD neuroinflammatory responses [15]. Persistent activation of the NF-κB pathway promotes the sustained production of pro-inflammatory factors, thereby accelerating neuronal damage and exacerbating AD pathogenesis. Collectively, these lines of evidence highlight the potential implication of mGluR5 in AD pathogenesis and suggest that targeting mGluR5 may be a promising therapeutic strategy for AD.

The phenolic compound ferulic acid (FA) is an active component found in traditional Chinese medicines such as *Ligusticum chuanxiong* and *Angelicae Sinensis Radix*, and it exhibits various pharmacological effects, including anti-inflammatory effects [16], antioxidant effects [17], cardioprotective effects [18], and hepatoprotective effects [19]. In our previous study, we observed that FA could cross the blood-brain barrier (BBB), and accumulate at high relative contents in the serum and brain tissues of 3×Tg-AD mice following systemic administration [20].

In the present study, we demonstrated that FA intervention could inhibit the activation of inflammatory microglia, reduce Aβ deposition and phosphorylation of tau protein, and ameliorate neuroinflammation by modulating the mGluR5/CaMKII/NF-κB pathway, while simultaneously improving cognitive impairment in 3×Tg-AD model mice. Our results highlighted the critical role of mGluR5 in regulating microglia-mediated neuroinflammation and emphasized the potential of FA as an mGluR5 agonist for AD treatment.

Materials and methods

Reanalysis of RNA sequencing datasets

RNA sequencing datasets were downloaded and screened for the expression level of GRM5 in AD condition, including 2 human bulk RNA sequencing datasets (GSE125583 and GSE125050 [21]), 2 human single nucleus RNA sequencing datasets (EC and SFG samples from GSE147528 [22] and MTG samples from GSE188545 [23]), and 2 mouse single nucleus RNA sequencing datasets (5×FAD samples from GSE140511 [24] and APP/PS1ΔE9 samples from GSE171095 [25]). All data was analyzed in R (4.3.1). For bulk RNA sequencing, the differential expression analysis was performed using DESeq2 [26], and the data was visualized using the R package ggplot2 [27] with several extension package (Heatmap [28] and ggdist [29]).

For snRNA-seq, the files were collected from GEO database, and the raw count matrices were analyzed using R package Seurat V5 [30]. After quality control with nFeature_RNA, nCount_RNA and percentage of mtRNA, samples were integrated with Harmony [31] algorithm using default parameters. Cell clusters were annotated with cell-type specific marker genes: human microglia (P2RY12, CSF1R and CX3CR1) and mouse microglia (Dock2, Csf1r, C1qa, P2ry12). After annotation, microglia were subset for further differential expression analysis with single cell specific algorithm, MAST [32].

Cell culture and MTT cell viability assay

Murine microglia (BV2) cells were obtained from iCell Bioscience Inc, and were cultured in DMEM (Gibco) containing with 10% FBS (Gibco) and 1% penicillin-streptomycin (Gibco). Cells were routinely maintained at 37℃ in humidified air containing 5% CO_2.

Cell viability was evaluated using the 3-(4,5-dimethylthiazol-2-yl)-2,5- diphenyltetrazolium bromide (MTT) assay kit. BV2 cells were treated with different concentrations of LPS or FA. Following 24 h of incubation at 37℃ with 5% CO_2, the culture supernatant was carefully aspirated, and 5 mg/mL MTT staining solution was added to each well. Cells were then incubated in the dark at 37℃ for 4 h to allow formazan crystal formation. After incubation, the MTT staining solution was removed, and dimethyl sulfoxide (DMSO) was added to each well to dissolve the formazan crystals. The absorbance of each well was measured at 570 nm using a universal microplate reader.

Animals and treatments

3×Tg-AD (APPSwe, tauP301L, PSEN1) transgenic mice were purchased from Nanjing University Nanjing Institute of Biomedicine, wild-type (WT) C57BL/6 mice were purchased from Hangzhou Medical College Experimental Animal Center (Hangzhou, China). The animals were kept at a constant room temperature and humidity in a 12 h light/12 h dark cycle with free access to tap water and food. All animal experiments in this study were reviewed and approved by the Hangzhou Medical College Animal Ethics Committee. The ethical approval number is 2024-012 (April 11, 2024).

Based on the human-equivalent dose conversion, the clinical adult oral dose of FA was 0.8 g/day, which was translated to a mouse-administered dose of 100 mg/kg/day. After one week of adaptation,

experimental mice were divided into six treatment groups (*n* = 8 per group): (1) WT mice treated with vehicle (WT group); (2) 3×Tg-AD mice treated with vehicle (3×Tg-AD group); (3) 3×Tg-AD mice treated with FA at 25 mg/kg/day (FA 25 mg/kg group); (4) 3×Tg-AD mice treated with FA at 50 mg/kg/day (FA 50 mg/kg group); (5) 3×Tg-AD mice treated with FA at 100 mg/kg/day (FA 100 mg/kg group); (6) 3×Tg-AD mice treated with DNPQ at 0.1 mg/kg/day (DNPQ group). All mice received intragastric gavage (i.g.) of vehicle, FA, or DNPQ once daily for a period of 2 months.

Western blotting

The microglial samples were lysed with RIPA buffer containing protease inhibitor and phosphatase inhibitor cocktail. Similarly, hippocampal and cortical tissues from mice were homogenized in RIPA buffer and kept on ice for 30 min. Following lysis or homogenization, the supernatants of samples were collected by centrifuging at 12000 × g for 15 min at 4℃, and protein concentrations were determined using a bicinchoninic acid (BCA) protein assay kit (Sangon, B5182510100). All protein samples were mixed with loading buffer and boiled at 95 ℃ for 10 min.

Protein samples were separated by SDS-PAGE gels and then transferred onto a PVDF membrane. After blocking at room temperature (RT) for 2 h, the membranes were incubated with primary antibodies overnight at 4℃. The following day, membranes were incubates with anti-rabbit or anti-mouse secondary antibodies at RT for 1 h. Protein bands were visualized using Gel Image System (Cytiva, 29399482) and quantified using Image J.

Immunofluorescence

For cellular immunofluorescent staining, cells were washed with phosphate-buffered saline (PBS) and fixed in 4% paraformaldehyde at RT for 20 min. For immunofluorescent staining of brain tissues, the brain slides were incubated with PBS containing 0.1% Triton X-100 (PBST) for 15 min. Then, all samples were blocked in 5% bovine serum albumin (BSA) at RT for 1 h, followed by incubation with primary antibodies overnight at 4℃. Subsequently, samples were washed with PBS and incubated with fluorescent secondary antibody for 1 h. Nuclei were stained with DAPI fluorescent dye (Servicebio, G1012). Fluorescent images were acquired by Leica SP8 confocal microscape and quantified using Image J.

Melacular docking and Cellular Thermal Shift Assay (CETSA)

The mGluR5 protein was obtained from the RCSB PDB database and molecular docking was performed using AutoDock software (1.5.7). Import the optimal docking results using the PyMOL software (2.6) and display the spatial interaction between FA and mGluR5.

CETSA evaluated in situ target-compound engagement with four biological replicates. BV2 cells were treated with FA or DMSO control for 2 h. Cells were lysed, aliquoted, heat-treated (40–60°C), centrifuged to collect soluble proteins. Equal protein amounts were analyzed by Western blot.

Flow cytometry

BV2 microglial cells were pretreated with various concentrations of LPS for 2 h and then treated with different concentrations of FA. Cell surface and intracellular markers were analyzed by multiparameter flow cytometry. Cells were incubated with CD86 antibody for 30 min at 4°C in the dark and washed with PBS containing 1% FBS. Data were acquired using a FACScan flow cytometer. Fluorescence compensation was performed with single-stained controls or compensation beads. Analysis was carried out using FlowJo software, with gating strategies determined by fluorescence-minus-one and isotype controls.

Nissl and HE staining

Nissl and HE staining were performed to detected neuronal nuclear in the hippocampus of WT and 3×Tg-AD mice. Nissl staining: Sections were incubated in 0.1% cresyl violet acetate (37°C, 10 min), rinsed with distilled water, differentiated in 95% ethanol, dehydrated in 100% ethanol, cleared in xylene, and mounted with neutral balsam. HE staining: Sections were stained with hematoxylin, tap water-rinsed to blue nuclei, differentiated in 1% hydrochloric acid-ethanol, rinsed, stained with eosin, gradient ethanol-dehydrated (95%, 100%), xylene-cleared, and mounted. Images of hippocampal CA1, CA3, and DG regions were observed at 40× magnifications. Nissl body-positive neurons and neuronal density were quantified using Image J.

RNA isolation and quantitative real-time PCR

Total RNA was isolation from mouse tissues using Trizol reagent. RNA underwent reverse transcription with PrimeScript RT reagent Kit (Takara, AP90652A). Quantitative real-time PCR was run and analyzed on LightCycler480 System (Roche, Switzerland). GAPDH served as the endogenous control, with relative expression levels calculated as fold changes vs. control groups.

Enzyme-linked immunosorbent assay (ELISA)

Brain samples were collected from WT and 3×Tg-AD mice and lysed with PBS buffer. Protein concentration was determined using a BCA Protein Assay Kit. The protein levels of IL-1β (JHN80300), TNF-α (JHN80536), Aβ40 (JHN80597) and Aβ40 (JHN80616), p-Tau 181 (JHN81038) and p-Tau 217 (JHN81094) were analyzed by ELISA kits in accordance with the manufacturer's protocols. All detections were performed at 450 nm using a multifunctional cellular imaging detection system.

Behavioral tests

Novel object recognition (NOR) test

The NOR test consisted of two consecutive days of experiments. On the first day, mice were placed into the apparatus containing two identical objects and allowed to freely explore these objects for 5 min. On the second day, one of the familiar objects was replaced with a novel object that differed in both shape and color, and the mice were then allowed to freely explore both objects for another 5 min. All behavioral data were collected for performance analysis, and the discrimination index (DI) was calculated to assess the recognition ability.

Morris water maze (MWM) test

The MWM test consisted of two phases. During the training phase, an invisible submerged platform was placed in a circular poor filled with opaque white water. Mice were then given 60 s to locate the platform and allowed to remain on it for 10 s. If a mouse failed to find the platform, it was gently guided and placed onto platform to remain 10 s. This training was conducted once daily for five consecutive days. On the sixth day, the platform was removed for the probe trial, and the mice were allowed to search the platform for 60 s. All experimental data was collected for performance analysis.

Statistical analysis

The two-sided unpaired Student's t-test was used to compare the difference between two independent samples. Group comparisons were performed by two-way ANOVA followed by Bonferroni's post hoc for multiple comparisons. All data were presented as means ± SEM, and $p < 0.05$ was considered statistically significant. Graphical presentations were developed with GraphPad Prism (version 9.0) software.

Results

mGluR5 was down-regulated in AD pathology and regulated microglia-mediated inflammation

We first interrogated the expression level of GRM5 upon Alzheimer's pathology. The expression level of GRM5 was decreased in the brain homogenate from patients with AD, and such association was independent of the gender. Further, we included the bulk RNA seq dataset using purified cells from AD patients or health controls, and expression level of GRM5 was significantly down-regulated in microglia, but not in astrocyte, neurons or endothelial cells (Fig. 1A). In the superior frontal gyrus (BA8) from patients with different Braak stage, single nuclei sequencing found a decrease in expression of GRM5 in microglia, which was significant comparing Braak stage 6 vs. 0. In the entorhinal cortex, advanced Braak stage showed a similar reverse association with the expression of GRM5 in microglia, though in a different pattern with SFG region (Fig. 1B). In the middle temporal gyrus region, the repression level of GRM5 was decreased in the microglia from AD patients. We then investigated the expression of GRM5 in microglia using datasets from transgenic mouse models, including 5×FAD and APP/PS1 mouse. Grm5 was expressed in a lower proportion of microglia, and the level was decreased significantly as well in

both models (Fig. 1C). Thus, both mouse and human datasets indicated that AD condition was associated with a decrease expression level of GRM5 in microglia.

Based on the above-mentioned facts, mGluR5 expressions in the hippocampus and cortex of 3×Tg-AD model mice aged 7–11 months were detected by Western blotting. The results showed that the protein levels of mGluR5 in these brain tissues of 3×Tg-AD mice were significantly decreased compared with those in WT mice (Fig. 1D-E). To further clarify the cellular localization and expression characteristics of mGluR5, immunofluorescence staining was used to analyze the mGluR5 effect in brain tissue sections and BV2 microglial cells, with microglia specifically labeled by Iba-1. As shown in Fig. 1F-K, mGluR5 was markedly down-regulated in the hippocampus and cortex of 3×Tg-AD mice, as well as in the LPS-induced BV2 cells. Moreover, the co-localization between mGluR5 and the microglial marker Iba-1 was significantly changed in these AD-related models (Fig. 1F and J), which reflected impaired functional coupling of mGluR5 in microglia during neuroinflammation.

The above results suggested that microglial mGluR5 was down-regulated in AD pathology, and this dysregulation may play a pivotal regulatory role in AD neuroinflammation.

FA suppressed pro-inflammatory microglial activation and ameliorated neuroinflammation by up-regulating mGluR5

Excessive activation of microglia disrupted their homeostatic balance and elicited the excessive release of cytotoxic mediators, which contributed to the propagation of neuroinflammatory cascades in pathological conditions [33, 34]. To establish an LPS-induced microglial neuroinflammation model, MTT (Fig. S1A-C) and flow cytometry assays (Fig. S1D-E) confirmed that the LPS concentration caused no significant BV2 cytotoxicity but markedly increased $CD86^+$ pro-inflammatory microglia, indicating successful model induction.

To investigate whether FA regulated microglial activation by targeting mGluR5, molecular docking and cellular thermal shift assay (CETSA) were first performed to verify the direct binding between FA and the mGluR5 protein [35]. Subsequently, the expression levels of mGluR5 and Iba-1 were evaluated in BV2 cells, as well as in the mice hippocampal and cortical tissues across different treatment groups, both *in vitro* and *in vivo*. Molecular docking results revealed a direct interaction between FA and mGluR5, with a high binding energy score (Fig. 2A). Furthermore, CETSA results showed that cell lysates from FA-treated group exhibited greater stability compared to the vehicle control group (Fig. 2B), thus confirming that FA bond to mGluR5 and stabilized the membrane-localized mGluR5 protein level.

Immunofluorescence staining results revealed that FA treatment significantly up-regulated mGluR5 expression and down-regulated Iba-1 protein levels in both *in vitro* (Fig. 2C-E) and *in vivo* models (Fig. 2H-L). Consistent with this observations, flow cytometry analysis (Fig. 2F-G) and immunofluorescence staining (Fig. 3A-C) further corroborated these findings, showing that FA treatment significantly reduced the proportion of $CD86^+$ pro-inflammatory microglia in LPS-stimulated BV2 cells, which indicated a shift toward a less activated microglial phenotype.

Given that excessive microglial activation induced neuronal damage, HE staining and Nissl staining were used to assess neuronal structure. HE staining showed that the neuronal structures in various regions of the hippocampus had significantly improved, with regular arrangement, a notable reduction in nuclear shrinkage and deepening of staining, and clearly distinguishable cell morphology (Fig. 3D-E). Consistent with these findings, Nissl staining indicated that FA significantly improved the structure of hippocampal neurons in 3×Tg-AD mice. Neuronal arrangement became compact and orderly, with plump cell bodies, increased number and enhanced staining intensity of Nissl bodies. In addition, the vacuolization and nuclear pyknosis were alleviated, and the cellular outline and structure were clearer (Fig. 3F-G). Taken together, FA effectively ameliorated the morphological damage of hippocampal neurons in 3×Tg-AD mice.

Collectively, these findings demonstrated that FA exerted a neuroprotective effect against AD neuroinflammation by directly targeting and up-regulating mGluR5, thereby attenuating aberrant microglial activation and subsequent neuronal damage.

FA ameliorated Aβ and Tau pathology in 3×Tg-AD mice by targeting mGluR5

With respect to AD-associated biomarkers, plasma phosphorylated tau at serine 181 and 217 (p-tau-181, p-tau-217) are two well-recognized plasma biomarkers for AD, which reflect the progression of tau pathology in the brain [36, 37]. Meanwhile, the ratio of amyloid β42 (Aβ42) to amyloid β40 (Aβ40) in brain tissue correlates tightly with the deposition of Aβ plaques, another key pathological feature of AD [38, 39]. The immunofluorescence results showed that FA treatment improved the APP and P-Tau proteins in the hippocampus and cortex of the 3×Tg-AD mice (Fig. 4A-E).

ELISA results showed that FA induced a marked reduction in the plasma concentrations of p-tau181 and p-tau217, as well as the Aβ42/Aβ40 ratio in the hippocampus of 3×Tg-AD mice (Fig. 4F-H). In addition, to explore whether FA exerted its therapeutic effects by targeting mGluR5, we performed the Pearson's correlation analysis, which revealed that the mGluR5 protein level was negatively correlated with both the levels of the aforementioned AD biomarkers and the expression levels of APP and tau proteins (Fig. 4I-K).

Taken together, all these results suggested that FA effectively ameliorated AD pathology in 3×Tg-AD mice by targeting mGluR5, which in turn regulated the abnormal expression of APP/Tau and reduced the levels of AD biomarkers, including the Aβ42/40 ratio and plasma p-tau-181, p-tau-217.

FA inhibited neuroinflammation in 3×Tg-AD mice through mGluR5/CaMK□/NF-κB pathway

Protein-protein interaction analysis demonstrated that mGluR5 interacted with multiple AD-related targets, among which most of the top 20 interacting proteins were associated with inflammatory responses, especially those involved in the NF-κB signaling pathway (Fig. 5A-B). Previous studies have

confirmed that mGluR5 regulates calmodulin expression, and our protein-protein interaction analysis further verified that mGluR5 may modulate the CaMK□/NF-κB pathway to ameliorate neuroinflammation in AD. To verify the regulatory relationship between mGluR5 and the CaMKII/NF-κB pathway, calcium imaging and immunofluorescence assays were performed, and the results demonstrated that an mGluR5 agonist promoted calcium influx and suppressed NF-κB nuclear translocation, whereas an mGluR5 antagonist reduced calcium influx and facilitated NF-κB nuclear translocation (Fig. 5C-F). To further elucidate the interrelationship between pathway molecules and inflammatory factors, Pearson's correlation analysis was performed across *in vitro* samples. The results showed significant positive correlations between mGluR5 expression and the levels of p-CaMK□, as well as a significant negative correlation between the expression of mGluR5 and the level of p-NF-κB p65 (Fig. 5G-I).

To investigate whether FA modulates the molecular mechanism underlying AD neuroinflammation through the mGluR5/CaMK□/NF-κB pathway, we first verified the regulation effect of FA against this pathway in 3×Tg-AD mice. Western blotting results showed that FA treatment effectively up-regulated the protein levels of mGluR5 and p-CaMK□, while down-regulated that of iNOS and p-NF-κB in both the hippocampus (Fig. 6A-E) and cortex of 3×Tg-AD mice (Fig. 6F-J). Additionally, qRT-PCR analysis revealed that FA administration significantly reduced the mRNA expression levels of the IL-1β and TNF-α and CD86 in the hippocampal and cortical tissues of mice (Fig. 6K). This observation further confirmed that FA-mediated inhibition of the mGluR5/CaMK□/NF-κB pathway translates to attenuation of neuroinflammatory responses *in vivo*.

All these data collectively indicated that promotion of mGluR5 expression by FA directly regulated the activation of the downstream CaMK□/NF-κB signaling pathway, which in turn mitigated neuroinflammatory cascades in the AD brain. This mechanistic insight provided robust support for the therapeutic efficacy of FA in 3×Tg-AD mice.

FA inhibited LPS-induced neuroinflammation in BV2 cells through the mGluR5/CaMK□/NF-κB Pathway

As we have determined that FA suppressed inflammatory activation through mGluR5/CaMK□/NF-κB pathway *in vivo*, we next further explored this mechanism *in vitro* inflammatory model of LPS-stimulated BV2 microglial cells. Calcium fluorescence imaging showed that LPS decreased the intracellular calcium level in BV2 cells, while FA treatment alleviated this LPS-induced calcium dysregulation, indicating that FA could normalize early calcium signaling perturbations in activated microglia (Fig. 7A-B).

Given that intracellular calcium dysregulation is a upstream trigger of NF-κB pathway activation, NF-κB serves as a crucial nuclear transcription factor, and its phosphorylated active form translocates into the nucleus to initiate the expression of pro-inflammatory factors [40], we next investigated whether FA-mediated modulation of calcium signaling would impact NF-κB activity. Immunofluorescence staining showed that LPS promoted NF-κB nuclear translocation, and FA treatment significantly inhibited such LPS-induced effect on NF-κB (Fig. 7C-E, Video1). Consistently, Western blot results showed that FA treatment remarkably up-regulated the protein expression levels of mGluR5 and p-CaMK□, while

decreased iNOS and p-NF-κB protein levels in BV2 cells (Fig. 7F-J). Specifically, the regulation of p-CaMK□ and p-NF-κB directly reflected the inhibition of pathway activation, while the reduced iNOS expression further confirmed the attenuation of pro-inflammatory responses in BV2 cells.

Consistent with these pathway-related observations, FA treatment also substantially decreased the mRNA expression levels of the pro-inflammatory cytokines IL-1β, TNF-α and CD86 in BV2 cells, while increased the mRNA level of CD206 (Fig. 7K). All results indicated that FA inhibited LPS-induced activation of CaMK□/NF-κB by increasing mGluR5.

FA ameliorated cognitive impairment in 3×Tg-AD mice by targeting mGluR5

Next, behavioral tests were performed to assess the potential of FA in ameliorating memory and cognitive impairments in 3×Tg-AD mice. The NOR and MWM tests were administered at baseline (prior to FA treatment), as well as 1 and 2 months treatment to evaluate the learning and memory abilities (Fig. 8A, Fig. S2A-E). Notably, FA treatment exerted dose and time-dependent beneficial effects. In the NOR test, compared with the 3×Tg-AD group, FA-treated mice showed a significant improvement in Discrimination Index (DI). Relative to their respective 1-month values, the DI increased by 21.9% in the 50 mg/kg group and 34.7% in the 100 mg/kg group at 2 months treatment, along with prolonged exploration time of the novel object (Fig. 8B-C, G-H).

The MWM test further validated this result. The movement trajectories of the six groups of mice showed that the average escape latency of FA-treated mice was significantly lower than that of 3×Tg-AD mice. Compared to their 1-month treatment result, the 50 mg/kg and 100 mg/kg FA groups showed a 31.1% and 39.2% reduction in escape latency at 2 months treatment, respectively (Fig. 8D, I). During the probe trial, FA-treated mice further demonstrated enhanced spatial memory by crossing the former platform location more frequently and spending a longer duration in the target quadrant compared to the model group (Fig. 8E-F, J-K).

Collectively, these data confirmed that FA significantly ameliorated cognitive impairment in 3×Tg-AD mice by regulating microglia mGluR5, with more pronounced effects observed after 2 months of treatment, and the 100 mg/kg dose exerting a superior therapeutic effect relative to 25 mg/kg and 50 mg/kg.

mGluR5 correlated with inflammatory cytokines and cognitive deficits in 3×Tg-AD mice after FA treatment

Finally, we investigated the association of mGluR5 with neuroinflammation and cognitive impairment in 3×Tg-AD mice after FA treatment. The results revealed that mGluR5 levels were positively correlated with the p-CaMK□/CaMK□ ratio (Fig. 9A), while the p-CaMK□/CaMK□ ratio was negatively correlated with the p-NF-κB/NF-κB ratio (Fig. 9B). These findings effectively confirm the reliability of the mGluR5/CaMK□/NF-κB pathway in 3×Tg-AD mice. Meanwhile, mGluR5 levels were negatively correlated with the levels of pro-

inflammatory cytokines IL-1 and TNF-α in the hippocampus of 3×Tg-AD mice after FA treatment (Fig. 9C). This further supported the regulatory role of mGluR5 in neuroinflammation mediated by the mGluR5/CaMK/NF-κB pathway, and also indicated that FA treatment does not disrupt the functional correlation of this pathway but rather modulated its activity to exert anti-inflammatory effects.

To evaluate cognitive function of 3×Tg-AD mice, we performed NOR and MWM test and found that mGluR5 and CaMK levels were positively correlated with the number of target platform crossings in the MWM test and the discrimination index in the NOR test, while being inversely correlated with the escape latency of mice on the last training day in the MWM (Fig. 9D-F, Fig. S3A-C).

Collectively, these comprehensive correlation analyses validated the reliability of the mGluR5/CaMK/NF-κB pathway and clarified that mGluR5 contributed to neuroinflammation and cognitive deficits in AD by regulating this pathway.

Discussion

The hypothesis regarding the signaling pathway mediated by mGluR5 has provided critical theoretical support for investigating the pathogenesis of AD [6]. Accumulating evidence has confirmed that mGluR5 activation serves as a central link connecting glutamatergic system dysfunction to AD-like pathological alterations in mice [41, 42]. However, the underlying potential downstream signaling mechanisms of the neuroprotective effect mediated by mGluR5 in AD remain unclear. Recent studies mainly focused on the regulatory role of mGluR5 in synaptic plasticity or the balance of glutamate metabolism [43, 44], while we explored the mechanism by which mGluR5 participates in the pathological regulation of AD from the perspective of its interaction with glial cells and the pro-inflammatory pathway of microglia. In the current study, we demonstrated that FA effectively activate mGluR5 and trigger the subsequent phosphorylation of CaMKII. Subsequently, this signaling process inhibited the nuclear transcriptional activity of NF-κB. All these molecular changes significantly alleviated neuroinflammatory responses, reduced Aβ plaque deposition, and abnormal phosphorylation of tau protein in AD mice.

In this study, our results revealed a marked down-regulation of mGluR5 protein expression in the hippocampus and cortical tissues of 3×Tg-AD mice, together with co-localization of this receptor with Iba-1, a specific maker of microglia. These results suggested that the reduced expression of mGluR5 in microglia was directly and causally related to the exacerbation of neuroinflammation in AD. The direct binding interaction between mGluR5 and FA was likely to stabilize the protein structure of mGluR5, prevent its degradation, or enhance its transcriptional activity, thereby restoring its regulatory function on microglial activation. Consequently, the rebound in mGluR5 expression was a key upstream event for FA to exert its anti-AD effect, providing direct experimental evidence for FA to intervene in AD neuroinflammation by targeting mGluR5 (Fig. 10).

Neuroinflammation serves as a critical pathological driver in the progression of AD, and sustained activation of the nuclear transcription factor NF-κB plays a central role in promoting inflammatory cascades [45]. Our research results indicated that the FA intervention significantly inhibited the

activation of the NF-κB pathway in the hippocampus and cerebral cortex of 3×Tg-AD mice. This result was fully supported by the reduced nuclear translocation level of p65 subunit and the significant down-regulation of the expression of pro-inflammatory cytokines. Notably, our mechanistic validation demonstrated that the inhibitory effect of FA on NF-κB pathway activation was mediated through the mGluR5/CaMKII pathway. Specifically, FA-induced activation of mGluR5 promoted intracellular calcium influx and further triggered the phosphorylation of downstream CaMKII protein. Our research results revealed that CaMKII, as a key effector molecule downstream of mGluR5, participated in its inhibitory effect on the activation of the NF-κB pathway. This discovery provided a novel molecular mechanism for anti-inflammatory effects of mGluR5 agonists in AD treatment and further refined the theoretical framework of mGluR5-related signaling pathway in regulating AD pathogenesis.

The current drugs or monoclonal antibodies targeting Aβ or tau have shown limited efficacy in clinical applications, indicating that the pathological process of AD is extremely complex and requires a multi-targeted treatment strategy [46]. FA is a natural compound widely distributed in various plants. We demonstrated that FA treatment effectively reduced Aβ deposition in the hippocampus of 3×Tg-AD mice and significantly decreased the plasma levels of p-tau 181 and p-tau 217. These two phosphorylated tau isoforms were identified as sensitive and specific blood biomarkers for the diagnosis and progression monitoring of AD, and their plasma levels were closely associated with cerebrospinal fluid (CSF) biomarkers and cerebral tau pathology. Therefore, FA simultaneously ameliorated the core pathological events in AD, thus provided a novel candidate strategy for multitargeted therapy of this disease.

Despite the meaningful findings obtained in the present study, several limitations should be acknowledged. While we have confirmed the mGluR5/CaMKII/NF-κB pathway as the core mechanism of the neuroprotective effect of FA, it is still unclear whether FA functions through other downstream signaling pathways [47, 48]. Another limitation of this study is that we did not use mouse models with specific mGluR5 gene knockout in microglia to clarify the role of mGluR5 in neuroinflammation, and thus conditional gene knockout models should be established to make up for this deficiency and to clarify the specific role of microglial mGluR5 in FA-mediated anti-inflammatory and neuroprotective effects.

Conclusions

This study demonstrated that the therapeutic effects of FA were achieved by targeting the mGluR5/CaMKII/NF-κB signaling axis to suppress neuroinflammation and alleviate the core pathological hallmarks of AD. Our data indicated that up-regulation of mGluR5 inhibited the CaMKII/NF-κB signaling cascade, which in turn attenuated neuroinflammation, reduced Aβ plaque deposition and p-tau levels, and ultimately improved cognitive function. Collectively, our findings systematically illustrated the multi-target neuroprotective effects of FA as a specific mGluR5 agonist, and highlighted its promising therapeutic potential as a candidate agent for the treatment of AD.

Abbreviations

FA
Ferulic acid
AD
Alzheimer’s Disease
WT
Wild-type
Aβ
Amyloidβ
BBB
Blood-Brain Barrier
CNS
Central Nervous System
LPS
Lipopolysaccharides
mGluR5
Metabotropic glutamate receptor 5
CaMKII
Calcium/calmodulin-dependent protein kinase II
NF-κB
Nuclear Factor kappa-light-chain-enhancer of activated B cells
DMSO
Dimethyl Sulfoxide
PBS
Phosphate Buffered Saline
ELISA
Enzyme Linked Immunosorbent Assay
IL-1β
Interleukin-1β
TNF-α
Tumor Necrosis Factor alpha
CESTA
Cellular Thermal Shift Assay

Declarations

Ethics approval and consent to participate

The study was approved by the Hangzhou Medical College Animal Ethics Committee. The ethical approval number is 2024-012 (April 11, 2024).

Competing Interests

The authors have declared that no competing interest exists.

Author details

[1]School of Basic Medical Sciences and Forensic Medicine, Hangzhou Medical College, Hangzhou, China

[2]School of Pharmacy, Hangzhou Medical College, Hangzhou, China

[3]School of Public Health, Hangzhou Medical College, Hangzhou, China

Funding

This work was suppported by 2024 National Health Commission Scientific Research Fund- Zhejiang Province Health Key Science and Technology Plan Project (NO. WKJ-ZJ-2422) and Key Discipline Construction Project of Traditional Chinese Medicine in Zhejiang Province (NO. 2024-XK-13). A Project Supported by Scientific Research Fund of Zhejiang Provincial Education Department (NO. Y202456781). Basic Research Project of Hangzhou Medical College (NO. KYYB2024004). And the Key Disciplines of Zhejiang Province in Public Health and Preventive Medicine (First Class, Category A), Hangzhou Medical College.

Author Contribution

YXY, QRX and YJL were responsible for conceptualization and supervision of the study. TY, JZ, YYW, ZS, WL, YHW and LCZ conducted the experiments (Investigation). TY, JZ and YYW performed data curation and formal analysis and drafted the original manuscript. All authors participated in reviewing and editing the manuscript and approved the final version. All data were generated in-house and no paper mill was used. All authors agree to be accountable for all aspects of work ensuring integrity and accuracy.

Acknowledgments

Not applicable.

Data availability

No datasets were generated or analysed during the current study.

References

1. Butovsky O, Rosenzweig N, Kleemann KL, Jorfi M, Kuchroo VK, Tanzi RE, et al. Immune dysfunction in Alzheimer disease. Nat Rev Neurosci. 2026;27(3):196–218.
2. Cheng J, Dong Y, Ma J, Pan R, Liao Y, Kong X, et al. Microglial Calhm2 regulates neuroinflammation and contributes to Alzheimer's disease pathology. Sci Adv. 2021;7(35):eabe3600.
3. van Olst L, Simonton B, Edwards AJ, Forsyth AV, Boles J, Jamshidi P, et al. Microglial mechanisms drive amyloid-β clearance in immunized patients with Alzheimer's disease. Nat Med. 2025;31(5):1604–16.
4. Sun Z, Zhang X, So KF, Jiang W, Chiu K. Targeting Microglia in Alzheimer's Disease: Pathogenesis and Potential Therapeutic Strategies. Biomolecules. 2024;14(7):833.
5. Ebrahimi R, Bordbar S, Azad G, Davoody S, Mahmoudi M, Esmaeilpour K. Beyond Neuroinflammation: Microglia at the Crossroads of Amyloid, Tau, and Neurodegeneration in Alzheimer's Disease. Neurol Sci. 2025;46(11):5591–605.
6. Abd-Elrahman KS, Ferguson SSG. Noncanonical Metabotropic Glutamate Receptor 5 Signaling in Alzheimer's Disease. Annu Rev Pharmacol Toxicol. 2022;62:235–54.
7. Kim J, Lee J, Song H, Koo JW, Kang S. mGluR5 as a Potential Orchestrator of Astrocyte Interactions in Neurological Disorders. Neural Plast. 2025;2025:7259018.
8. Wang Y, Wang J, Chen X, Lin Z, You Z, He K, et al. Tau pathology is associated with postsynaptic metabotropic glutamate receptor 5 (mGluR5) in early Alzheimer's disease in a sex-specific manner. Alzheimers Dement. 2025;21(2):e70004.
9. Wang J, He Y, Chen X, Huang L, Li J, You Z, et al. Metabotropic glutamate receptor 5 (mGluR5) is associated with neurodegeneration and amyloid deposition in Alzheimer's disease: A $^{[18F]}$PSS232 PET/MRI study. Alzheimers Res Ther. 2024;16(1):9.
10. Chen Y, Zhang Y, Chen Q, Liu Y, Wei X, Wu M, et al. Inhibition of mGluR5/PI3K-AKT Pathway Alleviates Alzheimer's Disease-Like Pathology Through the Activation of Autophagy in 5XFAD Mice. J Alzheimers Dis. 2023;91(3):1197–214.
11. Spurrier J, Nicholson L, Fang XT, Stoner AJ, Toyonaga T, Holden D, et al. Reversal of synapse loss in Alzheimer mouse models by targeting mGluR5 to prevent synaptic tagging by C1Q. Sci Transl Med. 2022;14(647):eabi8593.
12. Avelar P, Morais TP, de Castro-Abrantes H, Armada-Moreira A, Gonçalves-Ribeiro J, Valente CA, et al. BDNF prevents amyloid-β-induced exacerbation of mGluR5-driven Ca^{2+} transients in astrocytes through TrkB-Tc activation. Cell Calcium. 2026;134:103119.
13. Lin Z, Sun M. Phytochemical regulation of CaMKII in Alzheimer's disease: A review of molecular mechanisms and therapeutic potential. Pharmacol Res. 2025;216:107790.
14. Kim S, Sohn S, Choe ES. Phosphorylation of GluA1-Ser831 by CaMKII Activation in the Caudate and Putamen Is Required for Behavioral Sensitization After Challenge Nicotine in Rats. Int J Neuropsychopharmacol. 2022;25(8):678–87.

15. Jiang H, Ashraf GM, Liu M, Zhao K, Wang Y, Wang L, et al. Tilianin Ameliorates Cognitive Dysfunction and Neuronal Damage in Rats with Vascular Dementia via p-CaMKII/ERK/CREB and ox-CaMKII-Dependent MAPK/NF-κB Pathways. Oxid Med Cell Longev. 2021;2021:6673967.
16. Zhou X, Chen X, Cheng X, Lin L, Quan S, Li S, et al. Paeoniflorin, ferulic acid, and atractylenolide III improved LPS-induced neuroinflammation of BV2 microglia cells by enhancing autophagy. J Pharmacol Sci. 2023;152(2):151–61.
17. Mei Z, Hong Y, Yang H, Cai S, Hu Y, Chen Q, et al. Ferulic acid alleviates high fat diet-induced cognitive impairment by inhibiting oxidative stress and apoptosis. Eur J Pharmacol. 2023;946:175642.
18. Li L, Huang K, Wang D, Yang D, Gao K, Tang J, et al. Chlorogenic acid and ferulic acid in SMYAD alleviate diabetic cardiomyopathy by inhibiting cardiac lipotoxicity via GCGR/PPARα and GCGR/AMPK pathways. Phytomedicine. 2025;143:156906.
19. Pandi A, Chakraborty B, Sen N, Kalappan VM. The hepatoprotective potential of ferulic acid against a spectrum of pharmaceuticals and toxic compounds. Arch Toxicol. 2025;99(5):2229–34.
20. Hou J, Wang X, Zhang J, Shen Z, Li X, Yang Y. Chuanxiong Renshen Decoction Inhibits Alzheimer's Disease Neuroinflammation by Regulating PPARγ/NF-κB Pathway. Drug Des Devel Ther. 2024;18:3209–32.
21. Srinivasan K, Friedman BA, Etxeberria A, Huntley MA, van der Brug MP, Foreman O, et al. Alzheimer's Patient Microglia Exhibit Enhanced Aging and Unique Transcriptional Activation. Cell Rep. 2020;31(13):107843.
22. Leng K, Li E, Eser R, Piergies A, Sit R, Tan M, et al. Molecular characterization of selectively vulnerable neurons in Alzheimer's disease. Nat Neurosci. 2021;24(2):276–87.
23. Zhang L, He CH, Coffey S, Yin D, Hsu IU, Su C et al. Single-cell transcriptomic atlas of Alzheimer's disease middle temporal gyrus reveals region, cell type and sex specificity of gene expression with novel genetic risk for MERTK in female. medRxiv [Preprint]. 2023:2023.02.18.23286037.
24. Zhou Y, Song WM, Andhey PS, Swain A, Levy T, Miller KR, et al. Human and mouse single-nucleus transcriptomics reveal TREM2-dependent and TREM2-independent cellular responses in Alzheimer's disease. Nat Med. 2020;26(1):131–42.
25. Spurrier J, Nicholson L, Fang XT, Stoner AJ, Toyonaga T, Holden D, et al. Reversal of synapse loss in Alzheimer mouse models by targeting mGluR5 to prevent synaptic tagging by C1Q. Sci Transl Med. 2022;14(647):eabi8593.
26. Love MI, Huber W, Anders S. Moderated estimation of fold change and dispersion for RNA-seq data with DESeq2. Genome Biol. 2014;15(12):550.
27. Wickham H. (2016). ggplot2: Elegant Graphics for Data Analysis. Springer-Verlag New York. ISBN 978-3-319-24277-4. https://ggplot2.tidyverse.org
28. Kolde R. (2025). pheatmap: Pretty Heatmaps. R package version 1.0.13. https://github.com/raivokolde/pheatmap

29. Matthew Kay. (2025). ggdist: Visualizations of Distributions and Uncertainty. R package version 3.3.3. https://mjskay.github.io/ggdist/
30. Hao Y, Stuart T, Kowalski MH, Choudhary S, Hoffman P, Hartman A, et al. Dictionary learning for integrative, multimodal and scalable single-cell analysis. Nat Biotechnol. 2024;42(2):293–304.
31. Korsunsky I, Millard N, Fan J, Slowikowski K, Zhang F, Wei K, et al. Fast, sensitive and accurate integration of single-cell data with Harmony. Nat Methods. 2019;16(12):1289–96.
32. Finak G, McDavid A, Yajima M, Deng J, Gersuk V, Shalek AK, et al. MAST: a flexible statistical framework for assessing transcriptional changes and characterizing heterogeneity in single-cell RNA sequencing data. Genome Biol. 2015;16:278.
33. Lana D, Magni G, Landucci E, Wenk GL, Pellegrini-Giampietro DE, Giovannini MG. Phenomic Microglia Diversity as a Druggable Target in the Hippocampus in Neurodegenerative Diseases. Int J Mol Sci. 2023;24(18):13668.
34. Guo M, Wang Z, Zhou X, Yu C, Wu J, Yu L, et al. Ciliatoside A attenuates neuroinflammation in Alzheimer's disease by activating mitophagy and inhibiting NLRP3 inflammasome activation. Phytomedicine. 2025;145:156928.
35. Tu Y, Tan L, Tao H, Li Y, Liu H. CETSA and thermal proteome profiling strategies for target identification and drug discovery of natural products. Phytomedicine. 2023;116:154862.
36. Courade JP, Zetterberg H, Höglinger GU, Dewachter I. The evolving landscape of Alzheimer's disease therapy: From Aβ to tau. Cell. 2025;188(26):7337–54.
37. Welikovitch LA, Mate de Gerando A, Khasnavis A, Bhavsar H, Meltzer JC, Buée L, et al. Tau, synapse loss and gliosis progress in an Alzheimer's mouse model after amyloid-β immunotherapy. Brain. 2025;148(4):1316–28.
38. Wang J, Huang S, Lan G, Lai YJ, Wang QH, Chen Y, et al. Translational Biomarker Research of AgIng and Neurodegeneration (TBRAIN). Diagnostic accuracy of plasma p-tau217/Aβ42 for Alzheimer's disease in clinical and community cohorts. Alzheimers Dement. 2025;21(3):e70038.
39. Palmqvist S, Whitson HE, Allen LA, Suarez-Calvet M, Galasko D, Karikari TK, et al. Alzheimer's Association Clinical Practice Guideline on the use of blood-based biomarkers in the diagnostic workup of suspected Alzheimer's disease within specialized care settings. Alzheimers Dement. 2025;21(7):e70535.
40. Wang Y, Chen J, Li S, Cai Z. Ginsenoside Rh3-induced neurotoxicity involving the IP3R-Ca^{2+}/NOX2/NF-κB signaling pathways. J Nat Med. 2025;79(4):791–806.
41. Abd-Elrahman KS, Hamilton A, Albaker A, Ferguson SSG. mGluR5 Contribution to Neuropathology in Alzheimer Mice Is Disease Stage-Dependent. ACS Pharmacol Transl Sci. 2020;3(2):334–44.
42. Mecca AP, McDonald JW, Michalak HR, Godek TA, Harris JE, Pugh EA, et al. PET imaging of mGluR5 in Alzheimer's disease. Alzheimers Res Ther. 2020;12(1):15.
43. Salardini E, O'Dell RS, Tchorz E, Nabulsi NB, Huang Y, Carson RE, et al. Assessment of the relationship between synaptic density and metabotropic glutamate receptors in early Alzheimer's disease: a multi-tracer PET study. Alzheimers Res Ther. 2025;17(1):98.

44. Wang J, Huang Q, He K, Li J, Guo T, Yang Y, et al. Presynaptic density determined by SV2A PET is closely associated with postsynaptic metabotropic glutamate receptor 5 availability and independent of amyloid pathology in early cognitive impairment. Alzheimers Dement. 2024;20(6):3876–88.
45. Li B, Wang L, Xiao Y, Wang Y, Wang Y, Peng Y, et al. Gastrodin Ameliorates Tau Pathology and BBB Dysfunction in 3xTg-AD Transgenic Mice by Regulating the ADRA1/NF-κB/NLRP3 Pathway to Reduce Neuroinflammation. Phytother Res. 2025;39(5):1996–2016.
46. Bregman N, Nathan T, Shir D, Omer N, Levy MH, David AB, et al. Lecanemab in clinical practice: real-world outcomes in early Alzheimer's disease. Alzheimers Res Ther. 2025;17(1):119.
47. Wang NY, Li JN, Liu WL, Huang Q, Li WX, Tan YH, et al. Ferulic Acid Ameliorates Alzheimer's Disease-like Pathology and Repairs Cognitive Decline by Preventing Capillary Hypofunction in APP/PS1 Mice. Neurotherapeutics. 2021;18(2):1064–80.
48. Verma H, Dhureja M, Yadav A, Yadav B, Rao R, Dhiman M, et al. An In Vivo C57BL/6 Mouse Study Demonstrating Fine-Tuning of Serum and Brain-Derived Exosomes Reveal Therapeutic Potential of Phytochemical Ferulic Acid Against Alzheimer's Disease. Mol Neurobiol. 2025;62(10):12963–83.

Figures

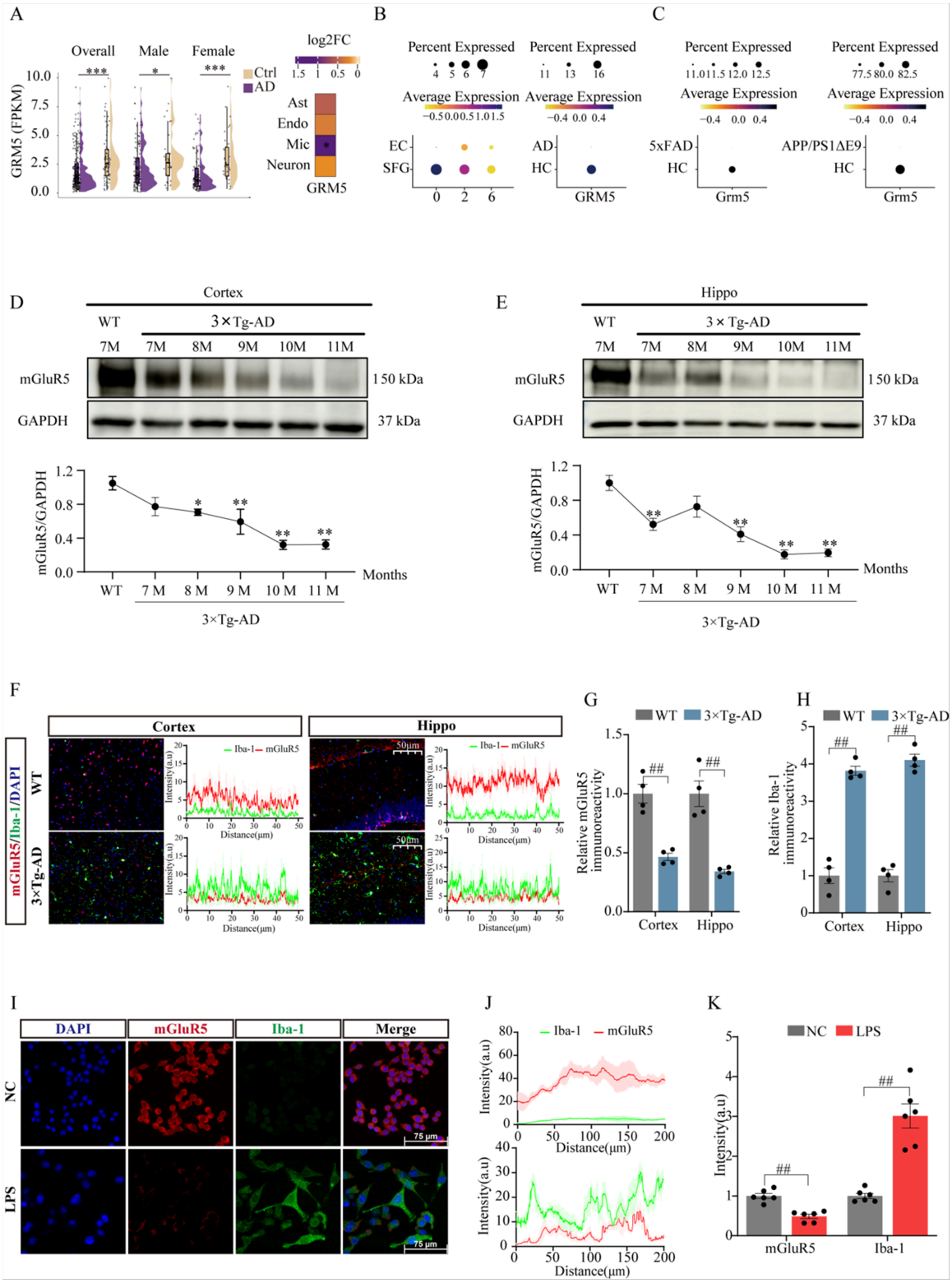


Figure 1

Microglial mGluR5 was down-regulated in AD pathology. **(A)** GEO datasets analyzed the expression level of GRM5 in the brain homogenate from AD patients. **(B)** GEO datasets analyzed the expression level of GRM5 in microglia. **(C)** GEO datasets analyzed the GRM5 in the microglia from AD patients and Grm5 in the microglia from 5×FAD and APP/PS1 mouse. **(D)** Western blot detected the protein levels of mGluR5 in the cortex of 7-month-old WT mice and 7-11 months 3×Tg-AD mice. **(E)** Western blot detected the

protein levels of mGluR5 in the hippocampus of 7-month-old WT mice and 7-11 months 3×Tg-AD mice. **(F-H)** Representative immunofluorescence images and its quantification of mGluR5 (G) and Iba-1 (H) in the hippocampus and cortex. Scale bar: 50 μm. **(I)** Representative immunofluorescence images of mGluR5 (red) and Iba-1 (green) in the BV2 cells. Scale bar: 75 μm. **(J)** The co-localization of mGluR5 and Iba-1 in the BV2 cells. **(K)** Quantification of mGluR5 and Iba-1 in the BV2 cells. All data were presented as mean ± SEM. **(D-E)** *n* = 6; **(F-H)** *n* = 4; **(I-K)** *n* = 6. **P* ⍰ 0.05, ***P* ⍰ 0.01; *##P* ⍰ 0.01.

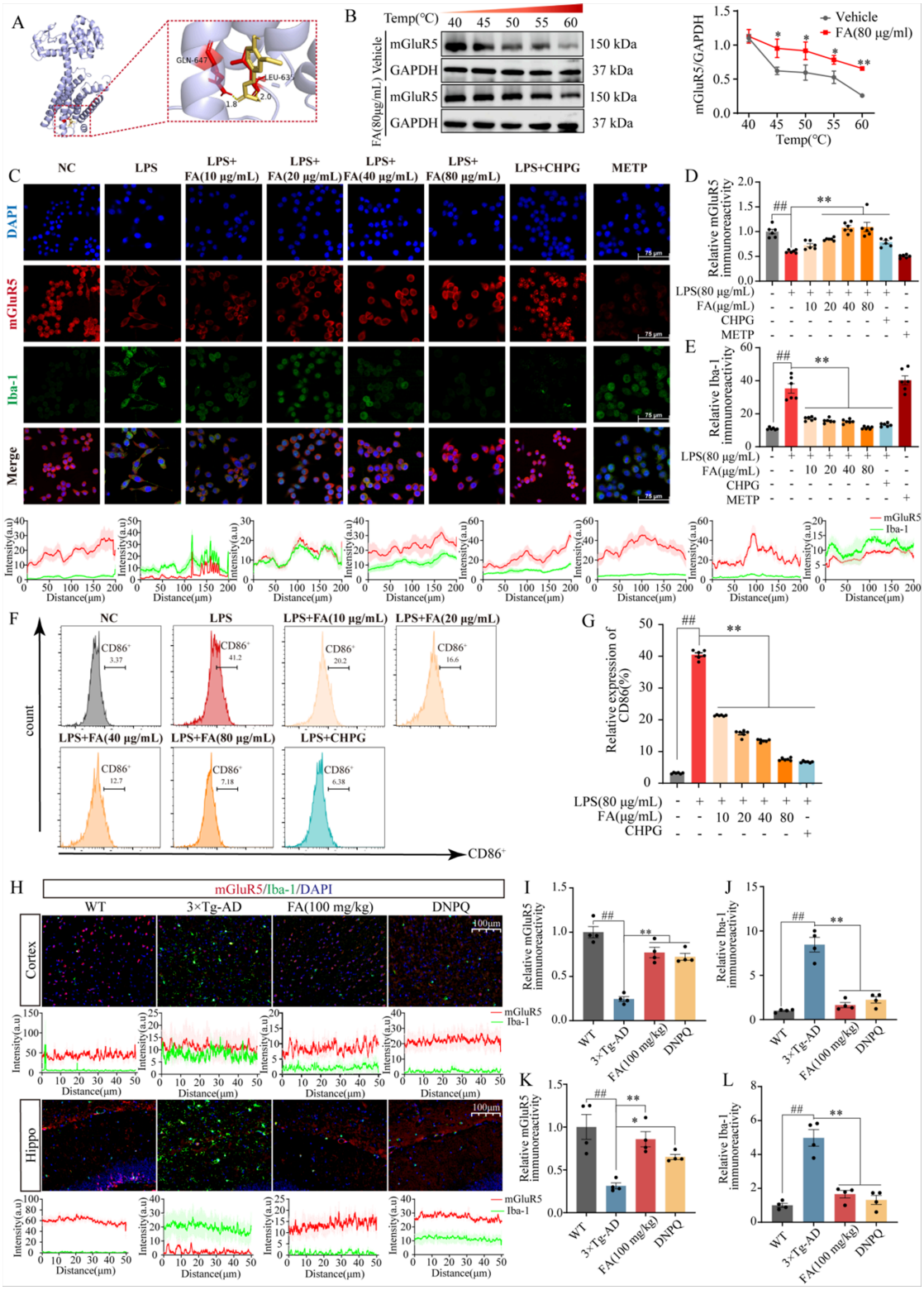


Figure 2

FA suppressed pro-inflammatory microglial activation by targeting mGluR5. **(A)** Molecular docking of FA with mGluR5. **(B)** CETSA detected the directly interaction between FA and mGluR5 in BV2 cells. **(C-E)** Representative immunofluorescence images and its quantification of mGluR5 (red) and Iba-1 (green) in the BV2 cells after FA treatment. Scale bar: 75 μm. **(F-G)** Flow cytometry detected the proportion of $CD86^+$ pro-inflammatory microglia in BV2 cells. **(H-L)** Representative immunofluorescence images and its quantification of mGluR5 (red) and Iba1 (green) in the hippocampus and cortex after FA treatment. Scale bar: 100 μm. All data were presented as mean ± SEM. **(A-B)** $n = 4$; **(C-G)** $n = 6$; **(H-L)** $n = 4$. $^{*}P < 0.05$, $^{**}P < 0.01$; $^{\#\#}P < 0.01$.

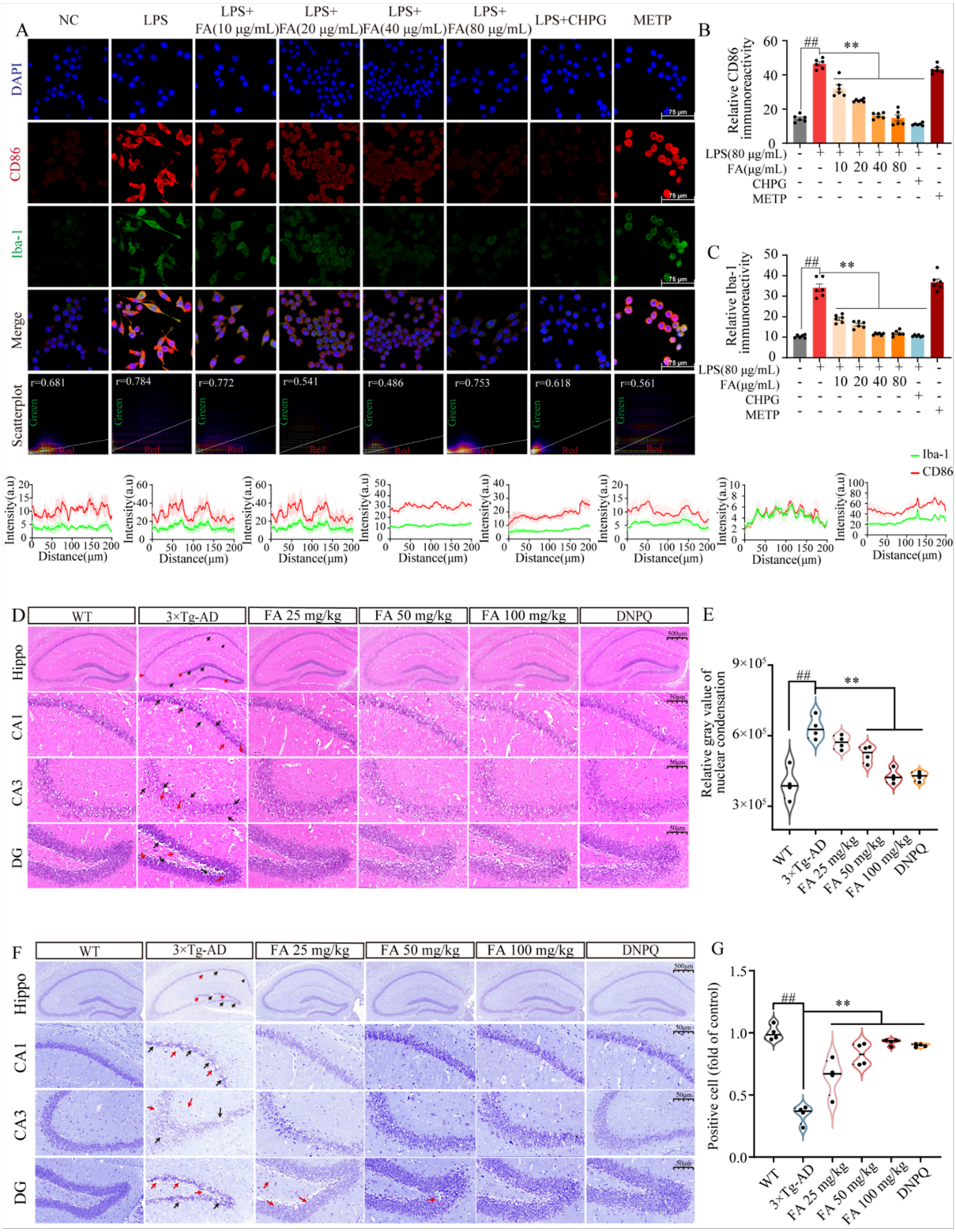


Figure 3

FA ameliorated hippocampal neuronal structure in 3×Tg-AD mice. **(A-C)** Representative immunofluorescence images and its quantification of CD86 (red) and Iba-1 (green) in the BV2 cells after FA treatment. Scale bar: 75 μm. **(D-E)** HE staining detected neuronal structures in various regions of the hippocampus in 3×Tg-AD mice. Scale bar: 500 μm (Hippo); 50 μm (CA1, CA2, DG). **(F-G)** Nissl staining

detected neuronal loss in the hippocampus of 3×Tg-AD mice. Scale bar: 500 μm (Hippo); 50 μm (CA1, CA2, DG). All data were presented as mean ± SEM. **(A-C)** *n* = 6; **(D-G)** *n* = 4. ***P* < 0.01; ##*P* < 0.01.

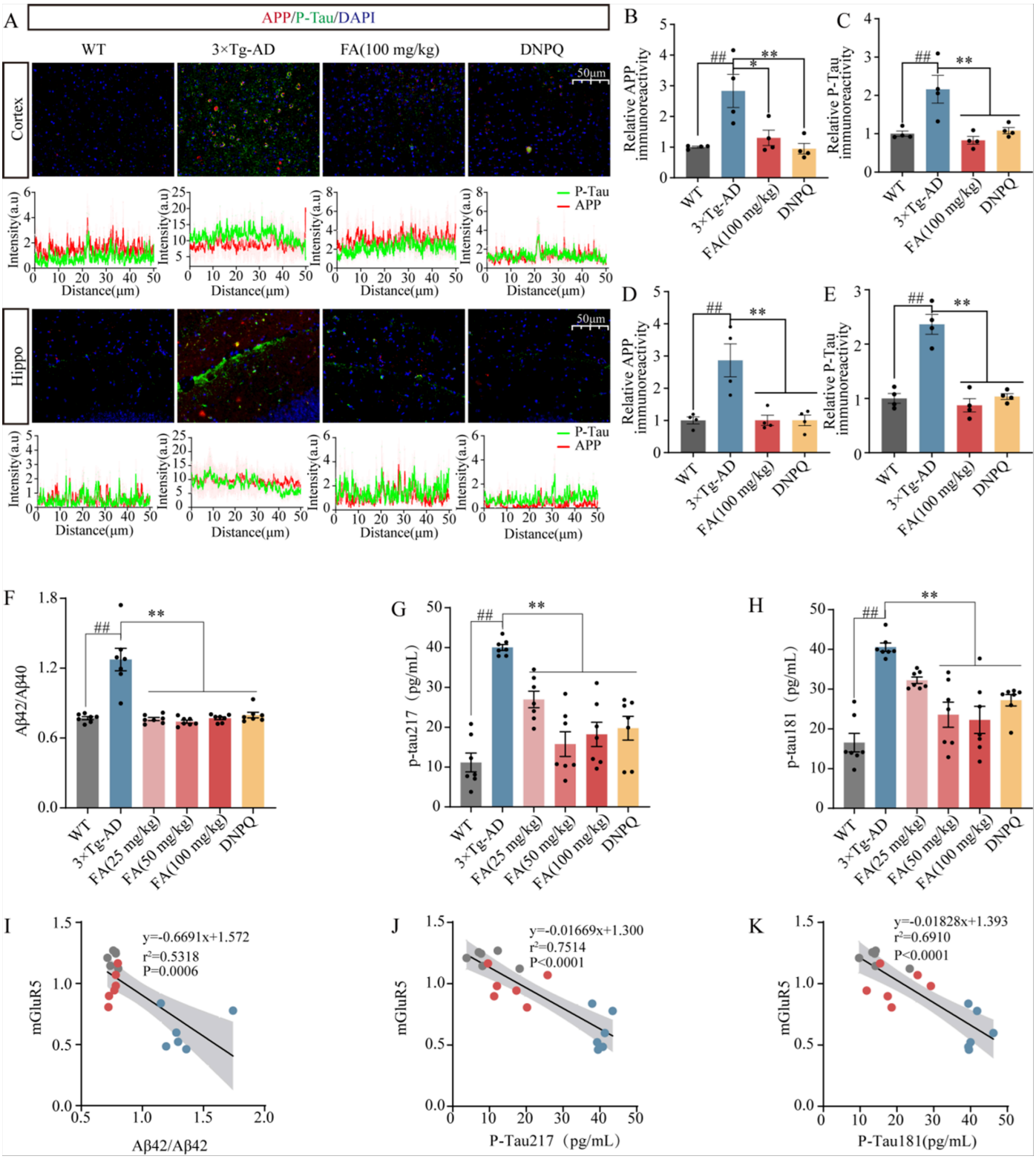


Figure 4

FA ameliorated Aβ and Tau pathology in 3×Tg-AD mice by targeting mGluR5. **(A)** Representative immunofluorescence images of APP (red) and P-Tau (green) in the hippocampus and cortex. Scale bar:

50 μm. **(B)** Quantification of APP in the cortex. **(C)** Quantification of P-Tau in the cortex. **(D)** Quantification of APP in the hippocampus. **(E)** Quantification of P-Tau in the hippocampus. **(F)** Aβ42/Aβ40 ratio in the hippocampus. **(G)** The protein levele of plasma p-tau-217. **(H)** The protein levele of plasma p-tau-181. **(I-K)** Correlation analysis between mGluR5 and (I) Aβ42/Aβ40 ratio, (J) plasma p-tau-217, (K) plasma p-tau-181. All data were presented as mean ± SEM. **(A-E)** *n* = 4; **(F-H)** *n* = 7; **(I-K)** *n* = 6. **P* < 0.05, ***P* < 0.01; ##*P* < 0.01.

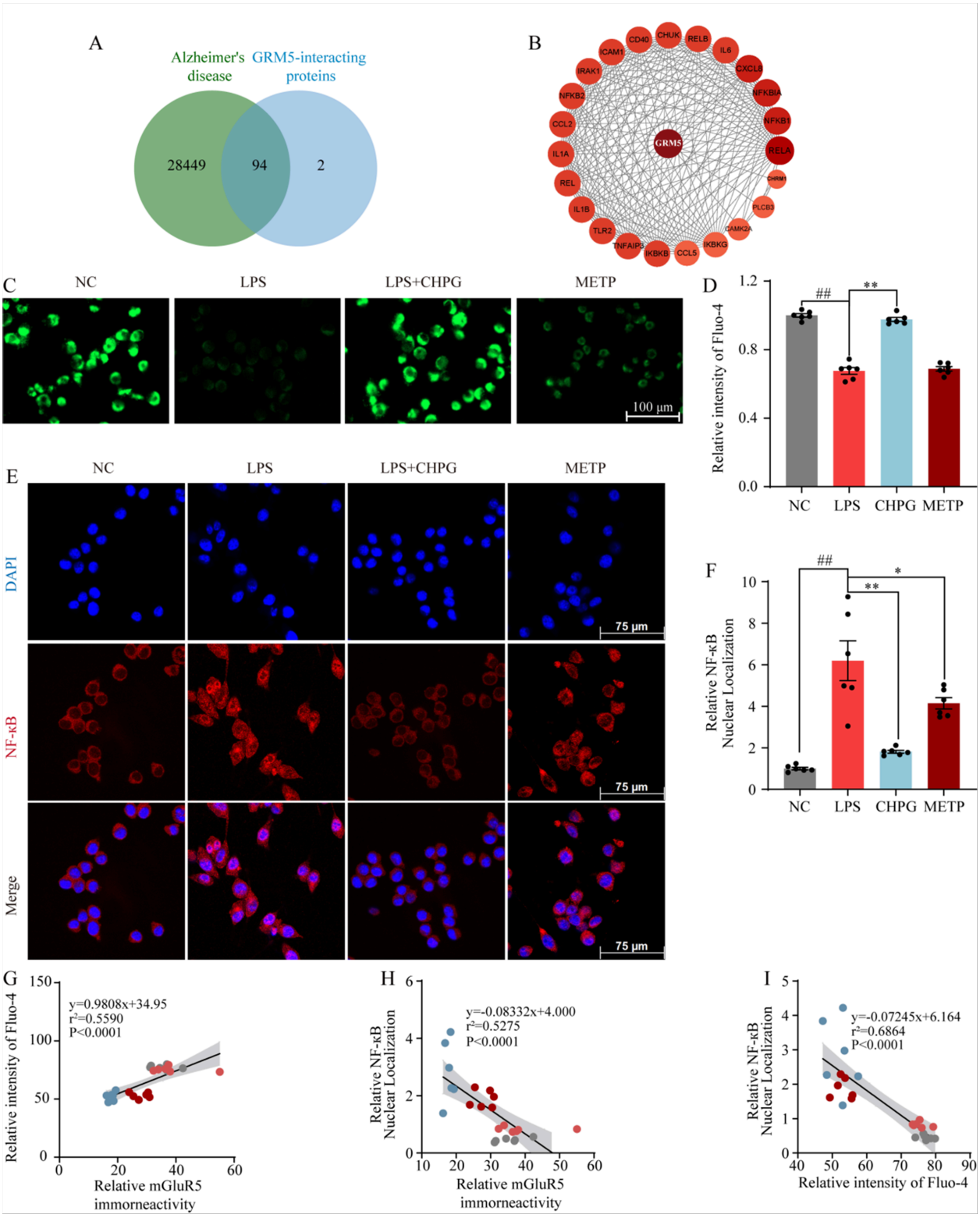


Figure 5

Protein interaction screening and validation of mGluR5 in improving the neuroinflammation regulatory pathway. **(A)** The Venn diagram of mGluR5 and AD proteins. **(B)** Protein-protein interaction between mGluR5 and AD-related targets. **(C-D)** Representative fluorescence images and its quantification of intracellular calcium level in the BV2 cells. Scale bar: 100 μm. **(E-F)** Representative immunofluorescence images and its quantification of NF-κB (red) in the BV2 cells. Scale bar: 75 μm. **(G)** mGluR5 levels positively correlate with levels of p-CaMK/CaMK. **(H)** p-CaMK/CaMK negatively correlate with levels of p-NF-κB/NF-κB. **(I)** mGluR5 levels negatively correlate with levels of p-NF-κB/NF-κB. All data were presented as mean ± SEM. n = 6. $^{\#\#}P$ 0.01; *P 0.05; **P 0.01.

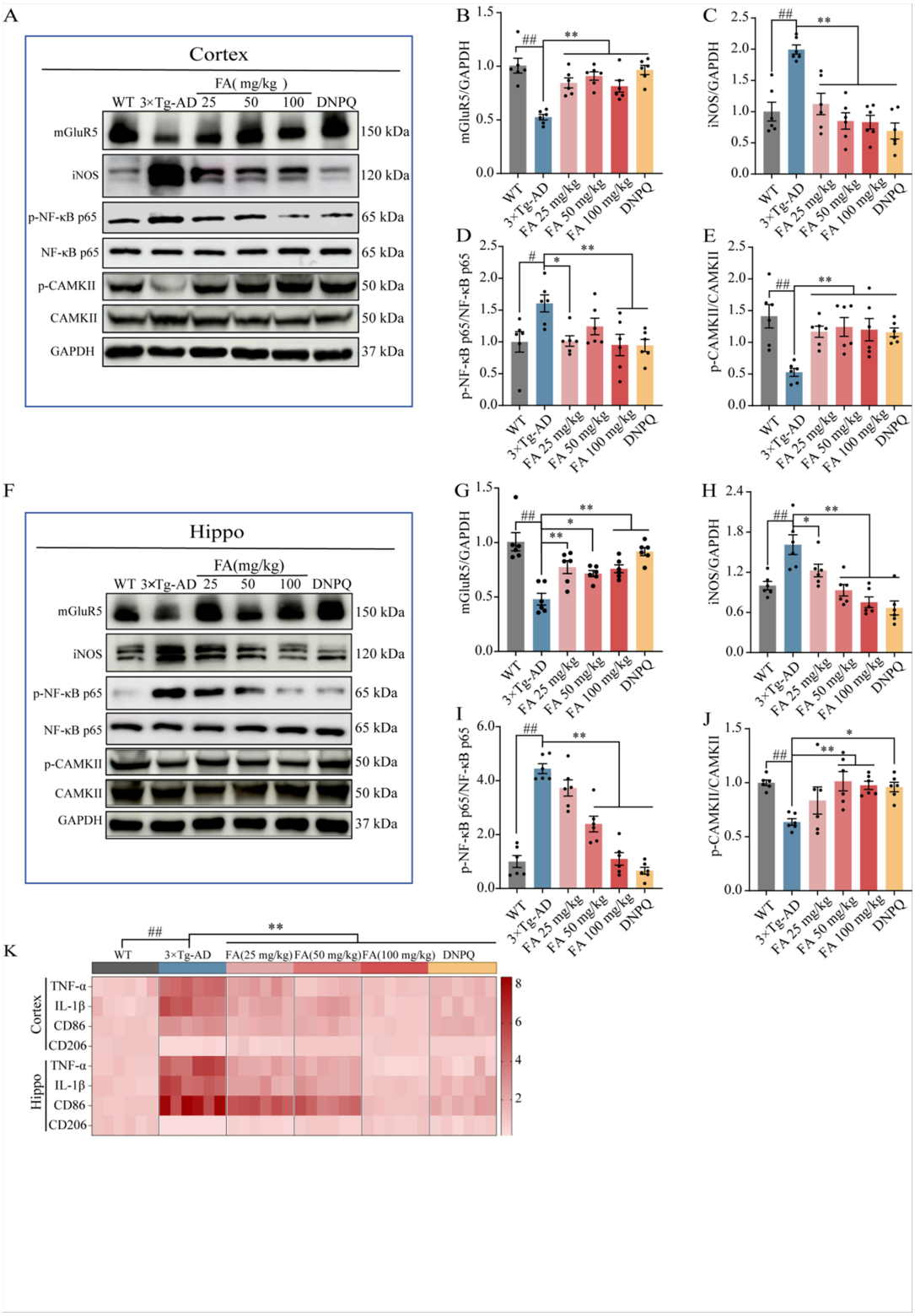


Figure 6

FA inhibited neuroinflammation in 3×Tg-AD mice through mGluR5/CaMK⍰/NF-κB pathway. **(A)** Western blot detected the protein levels of mGluR5, iNOS, p-CaMK⍰ and p-NF-κB in the cortex after FA treatment. **(B-E)** Quantification of relative protein levels in (A). **(F)** Western blot detected the protein levels of mGluR5, iNOS, p-CaMK⍰ and p-NF-κB in the hippocampus after FA treatment. **(G-J)** Quantification of

relative protein levels in (F). **(K)** qRT-PCR analysis of IL-1β, TNF-α, CD86 and CD206 mRNA levels in the cortex and hippocampus. All data were presented as mean ± SEM. *n* = 6. $^{\#\#}P$ < 0.01; *P < 0.05; **P < 0.01.

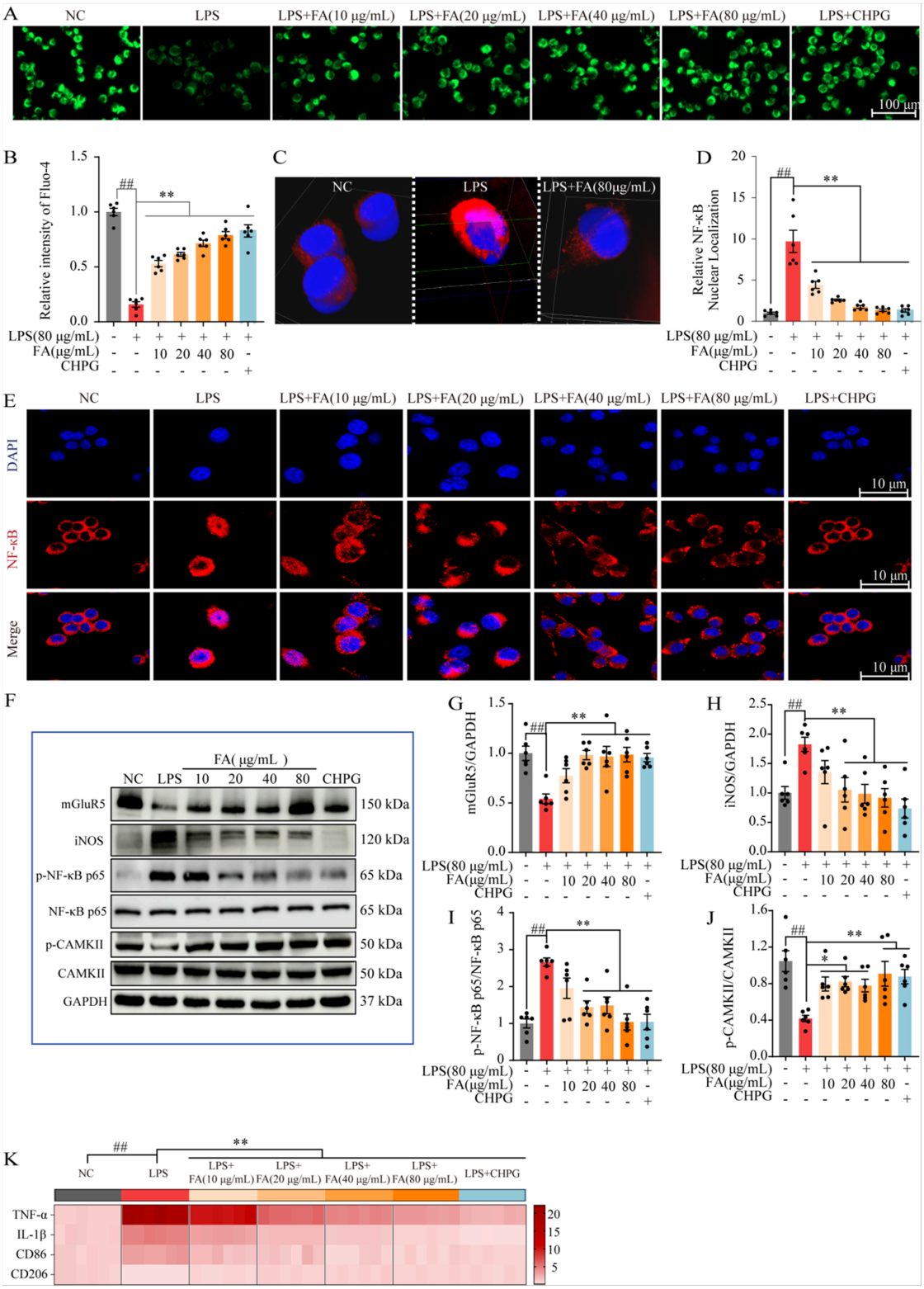


Figure 7

FA inhibited the neuroinflammation in BV2 cells through the mGluR5/CaMK⅁/NF-κB pathway. **(A-B)** Representative fluorescence images and its quantification of intracellular calcium level in the BV2 cells

after FA treatment. Scale bar: 100 μm. **(C-E)** Representative immunofluorescence images and its quantification of NF-κB (red) in the BV2 cells after FA treatment. Scale bar: 10 μm. **(F)** Western blot detected the protein levels of mGluR5, iNOS, p-CaMK and p-NF-κB in the BV2 cells after FA treatment. **(G-J)** Quantification of relative protein levels in **(F)**. **(K)** qRT-PCR analysis of IL-1β, TNF-α, CD86 and CD206 mRNA levels in the BV2 cells after FA treatment. All data were presented as mean ± SEM. *n* = 6. $^{\#\#}P$ 0.01; $^{**}P$ 0.01.

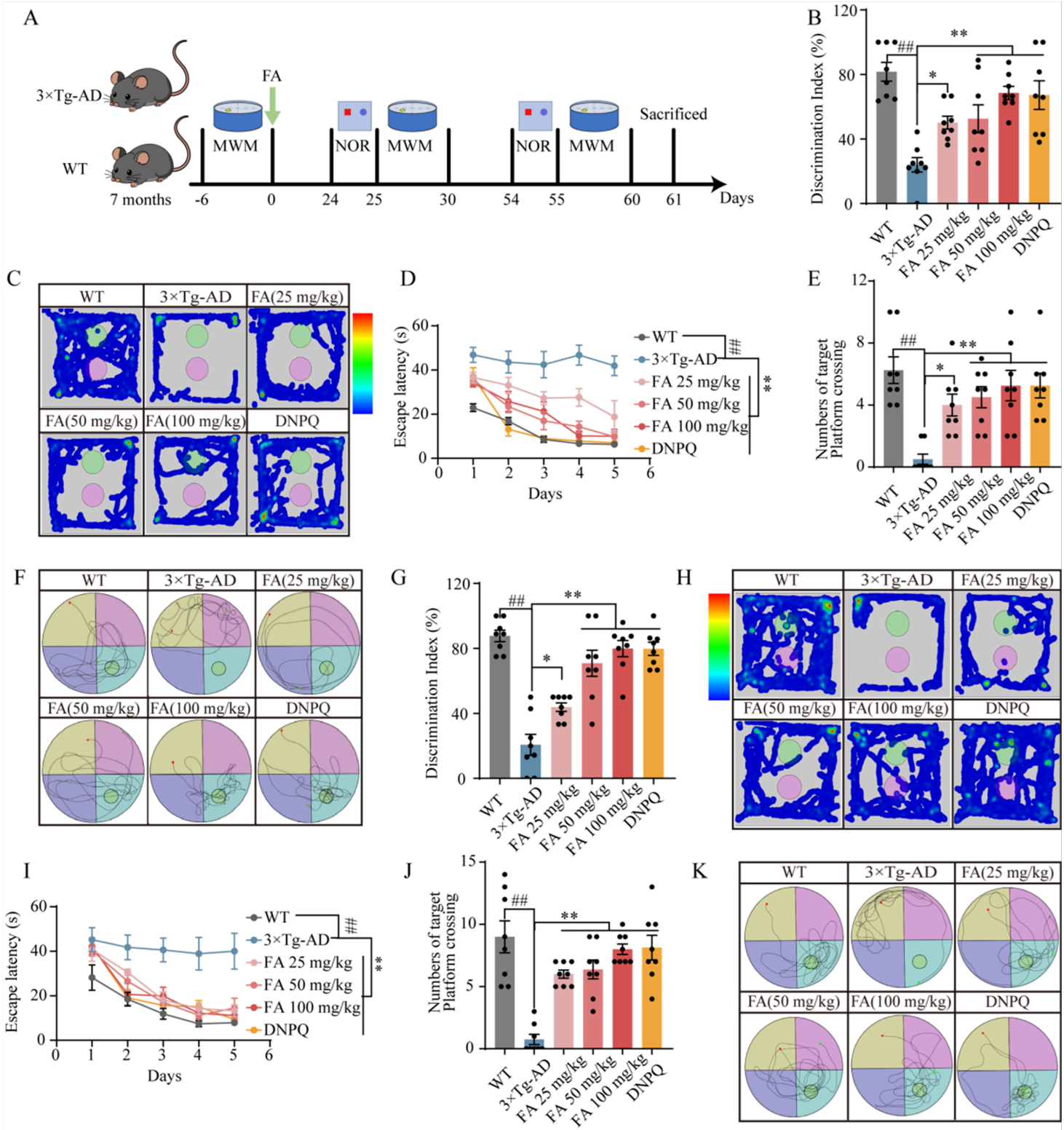


Figure 8

FA ameliorated cognitive impairment in 3×Tg-AD mice by targeting mGluR5. **(A)** Timeline of experimental procedure. **(B)** Discrimination index after 1 month of FA treatment in NOR test. **(C)** Representative trajectories of mice after 1 month of FA treatment in NOR test. **(D)** Escape latency after 1 month of FA treatment in MWM test. **(E)** Numbers of platform crossing in probe trials after 1 month of FA treatment in MWM test. **(F)** Representative swimming trajectories of mice after 1 month of FA treatment in MWM test. **(G)** Discrimination index after 2 months of FA treatment in NOR test. **(H)** Representative trajectories of mice after 2 months of FA treatment in NOR test. **(I)** Escape latency after 2 months of FA treatment in MWM test. **(J)** Numbers of platform crossing in probe trials after 2 months of FA treatment in MWM test. **(K)** Representative swimming trajectories of mice after 2 months of FA treatment in MWM test. All data were presented as mean ± SEM. n = 8. $^{\#\#}P$ < 0.05; $^{**}P$ < 0.01.

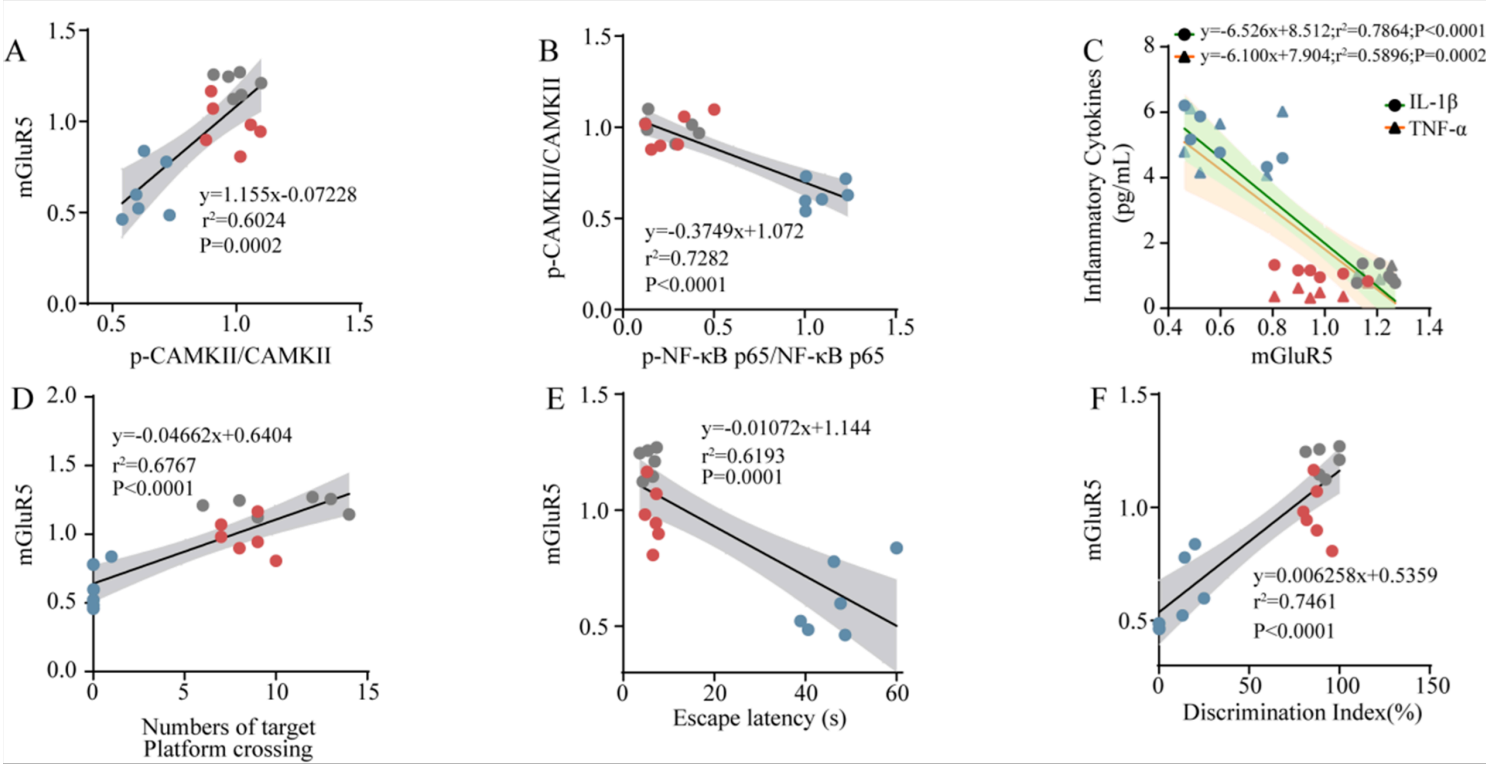


Figure 9

Correlations between mGluR5 and CaMK□/NF-κB, and inflammatory cytokines, and cognitive function in WT and 3×Tg-AD mice. **(A)** mGluR5 levels positively correlate with levels of p-CaMK□/CaMK□. **(B)** p-CaMK□/CaMK□ negatively correlate with levels of p-NF-κB/NF-κB. **(C)** mGluR5 levels negatively correlate with levels of IL-1β and TNF-α in brain samples of 3×Tg-AD mice. **(D)** mGluR5 levels positively correlate with numbers of target platform crossing of MWM test. **(E)** mGluR5 levels negatively correlate with escape latency on the last day of training in the MWM test. **(F)** mGluR5 levels positively correlate with discrimination index in the NOR test. n = 8. Correlations were analyzed by linear regression and Pearson's correlation coefficients.

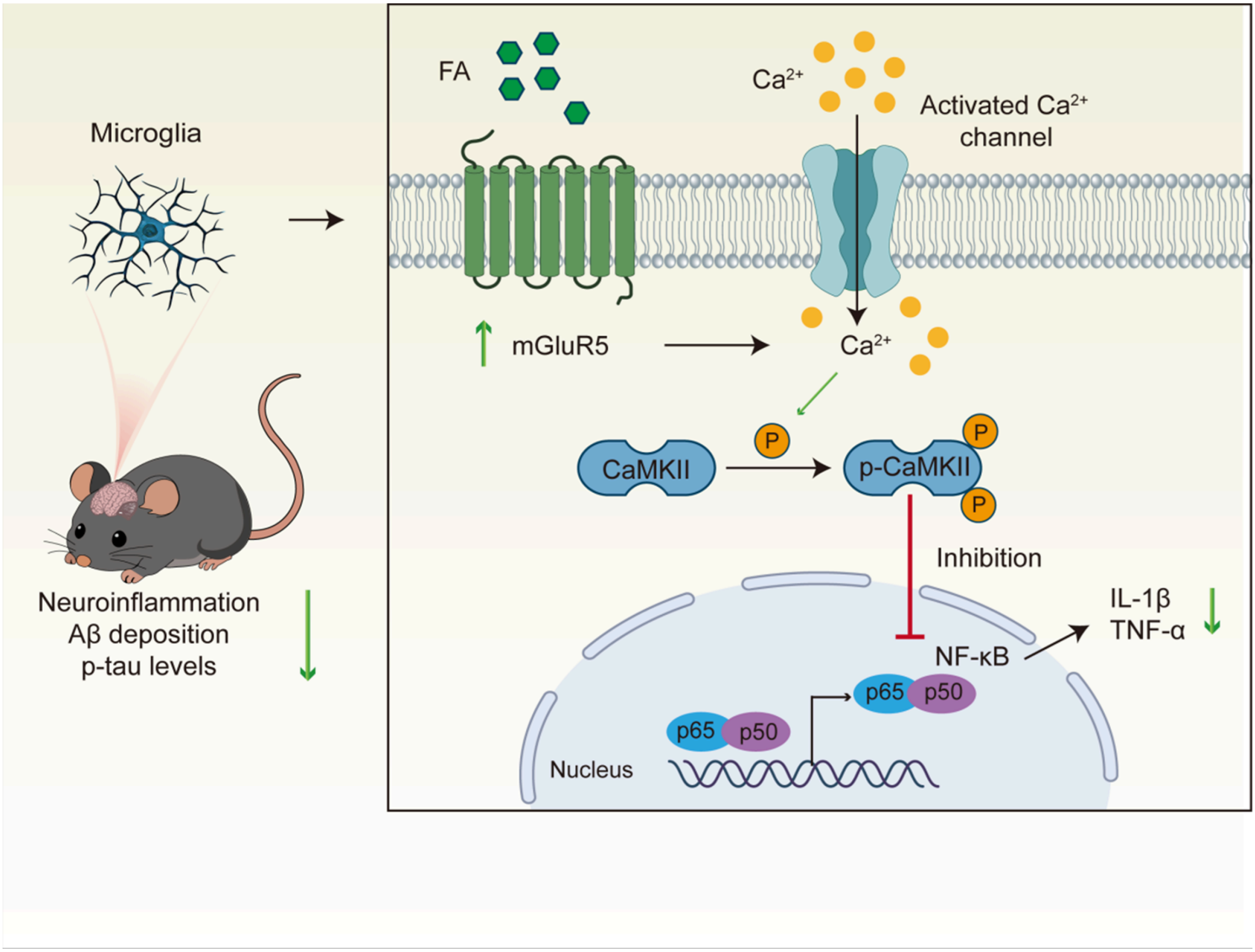


Figure 10

FA ameliorated pathological phenotypes and cognitive dysfunction in 3×Tg-AD mice by regulating microglial mGluR5/CaMK/NF-κB pathway to reduce neuroinflammation, Aβ and tau pathology.

Supplementary Files

This is a list of supplementary files associated with this preprint. Click to download.

- supplementaryfile.zip
- FulluncroppedGelsandBlotsimage.pdf
- image11.png
- image12.png
- image13.png